Materials Today: Proceedings 46 (2021) 638–644

Contents lists available at ScienceDirect

Materials Today: Proceedings

journal homepage: www.elsevier.com/locate/matpr

Effect of tool geometry on microstructure and mechanical properties of submerged friction stir processed AA6082/AA8011 joints

Velaphi Msomi *, Sipokazi Mabuwa, Oritonda Muribwathoho, Sharon S. Motshwanedi

Cape Peninsula University of Technology, Mechanical Engineering Department, Bellville 7535, South Africa

ARTICLE INFO

Article history:
Received 22 August 2020
Accepted 18 November 2020
Available online 19 January 2021

Keywords:
Friction stir welding
Friction stir processing
Microstructure
Ultimate tensile strength
Microhardness
Tool pin profile

ABSTRACT

This paper reports on the influence of the pin profile towards the microstructure and the mechanical properties of the underwater friction stir processed dissimilar (SFSP) AA6082/AA8011 joint. The friction stir processed (processed) dissimilar joints were initially produced through the friction stir welding technique. The SFSP joint produced using two different pin profiles were studied comparatively. The cylindrical threaded pin profile (TP1) and triangular pin profile with flutes (TP2) were used in performing SFSP on AA6082/AA8011 dissimilar joint. The joint produced using with TP2 pin profile had finer grains compared to the joint produced using the TP1 pin profile. The tensile properties of the joint produced with TP2 were higher compared to those produced using TP1.

1. Introduction

Friction stir processing (FSP) is known as one of the techniques which can improve the mechanical properties of metals [1]. FSP was derived from the well known joining technique called friction stir welding (FSW) [2]. The proper application of FSP technology depends on the good combination of various parameters i.e. tool pin profile, tool rotational speed, tool traverse speed, tool tilt angle, FSP conditions, etc [3–6]. The slight variation on any of these parameters will always have an impact on the properties of the friction stir processed (FSPed) surface [7,8]. Various works have been conducted in trying to understand the influence of various FSP parameters on the properties of surfaces and joints. Hamed et al. [9] have investigated the influence of FSP conditions on the corrosion behavior of AZ31B magnesium alloy. The rotational and traverse speed were the parameters that were varied in this study. It was discovered the increase in rotational speed contributed to the refinement of grain size. The increase in the number of FSP passes contributed further to the refinement of grains which also played a significant role in corrosion resistance.

Shalok et al. [10] have studied the impact of tool rotational speed on the mechanical properties of the FSPed AA5052 plate. The FSPed results were studied in comparison to the parent material. The hardness of the FSPed plate was found to be higher compared to the parent material. The wear resistance of the FSPed samples was found to be higher than that of the parent material. The increase in hardness value was found to have a good correlation with the wear rate. Ale et al. [11] studied the impact of heat treatment on the FSPed AA5052 plate. The application of heat treatment post FSP resulted in an increase in tensile strength, microhardness, and wear resistance. Ma et al. [12] have analyzed the influence of traverse speed on the behavior of 2507 duplex stainless steel. The tool rotational speed was kept constant while the traverse speed was being varied. It was discovered that the increase in traverse speed contributed to the refinement of grains in the stir zone which resulted in the increase in ultimate tensile strength and microhardness but reduced the elongation. It was further discovered that the grain refinement promoted the diffusion of elements and also the enhanced passivation film stability which contributed to the increase in corrosion resistance.

Kumar [13] has used the Taguchi method in optimizing the FSP tool profile that is suitable for the enhancement of the mechanical properties of the FSPed AA6061 plate. The three tool profiles were used in performing the Taguchi L9 method i.e. square threaded pin, cylindrical threaded, and cylindrical pin. The tool tilt angle and the traverse speed were the only two parameters that were varied. It was discovered that the square pin profile could give the maximum tensile strength when the rotational speed is 1400 rpm traversing at 60 mm/min and the tool tilted at an angle of 2°.

* Corresponding author.
E-mail address: msomiv@gmail.com (V. Msomi).

https://doi.org/10.1016/j.matpr.2020.11.580
2214-7853/

Table 1
Chemical composition of the as-received plate (wt.%) [3].

Material type	Mg	Zn	Ti	Cr	Si	Mn	Fe	Cu	Al
AA6082	1.1	0.2	–	0.25	0.9	0.7	0.5	0.1	Bal
AA8011	0.28	0.084	0.016	0.028	0.52	0.46	0.74	0.13	Bal

Table 2
Friction stir welding parameters.

Tool tilt angle (°)	Dwell time (s)	Rotational speed (rpm)	Traverse speed (mm/min)
2	10	1100	60

The influence of various FSP parameters on the behavior of the FSPed surface has not been reported extensively. The majority of works reported on the influence of the FSP parameters on a single surface but there are limited works that extend the FSP technique to joints. This work reports on the impact of the FSP pin profile on the microstructure and tensile strength of AA6082/AA8011 dissimilar joint that was processed underwater.

2. Materials and methods

The 6 mm thick AA6082-T6 and AA8011-H14 plates were cut into 250 mm × 70 mm to fit in the backing plate of the semi-automated milling machine. The chemical composition of the two aluminum alloys is presented in Table 1. The FSW technology was used to form the AA6082/AA8011 dissimilar joint. The parameters used in joining the two plates are presented in Table 2. The welded dissimilar plates were then subjected to FSP which was performed underwater using two different pin profiles i.e. cylindrical threaded pin and triangular profile with flutes. The photograph of the two tool pin profiles is presented in Fig. 1. The high carbon steel (H13) was used in manufacturing tool with a cylindrical threaded profile (TP1) while high-speed steel (HSS) was used in manufacturing tool with a triangular profile with flutes (TP2).

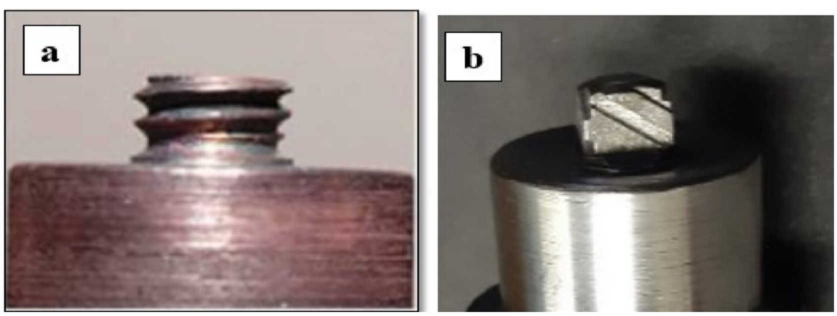

Fig. 1. Pin profiles (a) cylindrical threaded pin; (b) triangular profile with flutes.

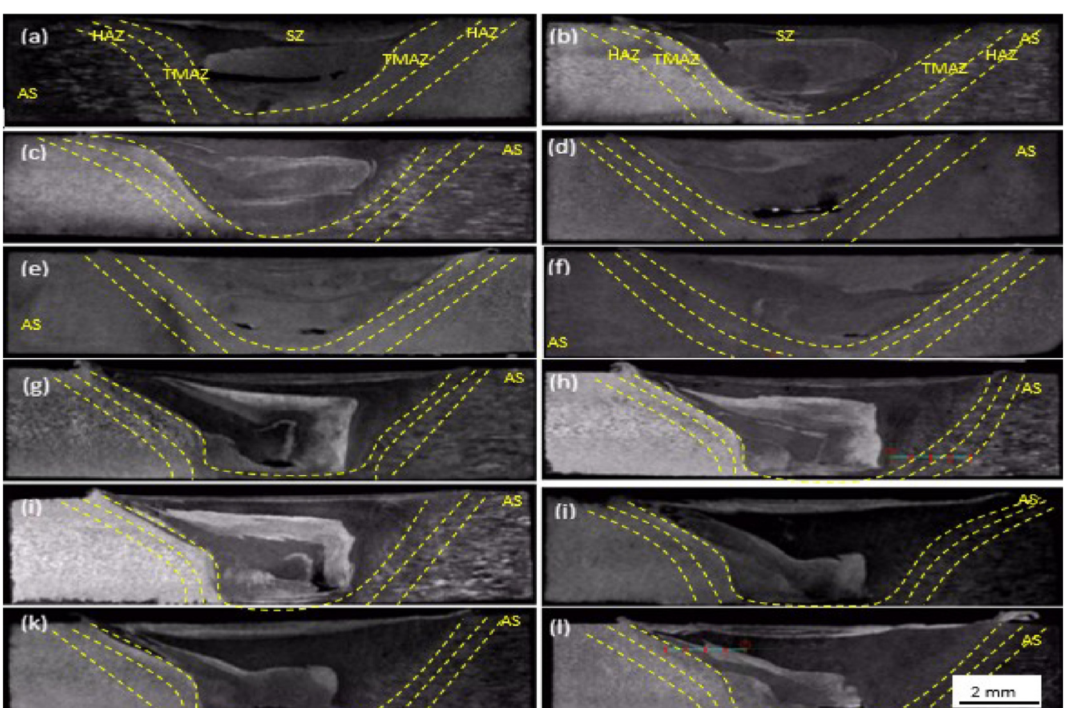

Fig. 2. Macrostructure: TP1, (a) 1pass- Start, (b) 1pass-Middle, (c) 1pass - End, (d) 2pass - Start, (e) 2pass - Middle and (f) 2pass - End; TP2, (g) 1pass - Start, (h) 1pass - Middle, (i) 1pass - End, (j) 2pass - Start, (k) 2pass - Middle and (l) 2pass - End.

The diameter of the tool shoulders was 20 mm while the diameter for the probes was made to be 7 mm and the length of the two pins was 5.8 mm. The parameters used for welding were similar to those utilized for the underwater friction stir processing. The AA6082 plate was kept constantly at the advancing side during FSW and underwater FSP. The 2pass FSP technique was used in performing the underwater FSP in each pin profile. The waterjet technology was used in preparing specimens for various tests.

Instron 8801 machine was used in performing the tensile tests and the tensile specimens were prepared based on the ASTM-E8M-04 standard. The post- tensile test specimens were further analyzed using the scanning electron microscopy (SEM). The ASTM E384-11 standard was used in performing microhardness tests on the InnovaTest Falcon 500 machine. The 10 s dwell time was employed in the performance of microhardness using the 500 g load. The microstructural analysis was performed using the Motic AE2000 microscope and the modified Keller's and Weck's agents were used to etch the specimens before the examination. It should be noted that the specimens were cut from different locations on each FSPed plate and this was because the mechanical properties vary across the joint [14]. The specimen that was cut from the beginning of the joint is labeled with S, M is used to label the specimen that was cut from the middle of the joint and E is the label used for specimen cut at the end of the joint. All the specimens were cut perpendicular to the FSP direction.

3. Results and discussions

3.1. Macrostructural analysis

Fig. 2(a) to (f) presents the macrographs of the underwater friction stir processed joint using TP1 while the macrographs for TP2 is shown in Fig. 2(g) to (l). The characteristics of dissimilar joint regions are visible from all macrographs i.e. heat-affected zone (HAZ), thermomechanical affected zone (TMAZ), and stir zone (SZ) also known as nugget zone. Moreover, the swirl marks underneath the shoulder which indicate the advancing and the retreating side are also visible in all the joints. It is good to note that the swirl marks shapes differ with tool profile i.e. the knee-like shaped swirl marks were produced when TP2 was used for submerged friction stir processing (SFSP) while the oval-like shaped swirl marks were produced when the SFSP was conducted using TP1 [15]. There are visible defect on the SZ for the 2pass SFSP joint for TP1 and this defect suggest inadequate mixing of materials. However, the defect size is larger for the specimens sampled at the beginning of the joint and getting smaller towards the end of the SFSP joint (see Fig. 2(d)-(f)). Additionally, these defects are all located towards the root surface (surface near the backing plate) of the joint. A similar defect was also observed from the specimen sampled at the start and the end of the 1pass SFSP joint (see Fig. 2 (g) & (i)) produced using TP1. A similar defect was also present on the specimens sampled from the middle and the end of the 2pass SFSP joint produced using TP2.

3.2. Microstructural analysis

The measurement of the mean grain size was performed using a linear intercept method through ImageJ software. Fig. 3(a)-(c) show the stir zone of 1pass SFSP AA6082/AA8011 joint while Fig. 3 (d)–(f) show the stir zone of 2pass SFSP AA6082/AA8011 joint and all these joints were produced using TP1. The stir zone of 1pass and 2pass SFSP AA6082/AA8011 joint is shown in Fig. 4(a)–(e), respectively. The mean grain size at the stir zone produced using TP1 was found to be in the range between 21.09 μm and 30.77 μm throughout the joint i.e. the start, middle, and end of

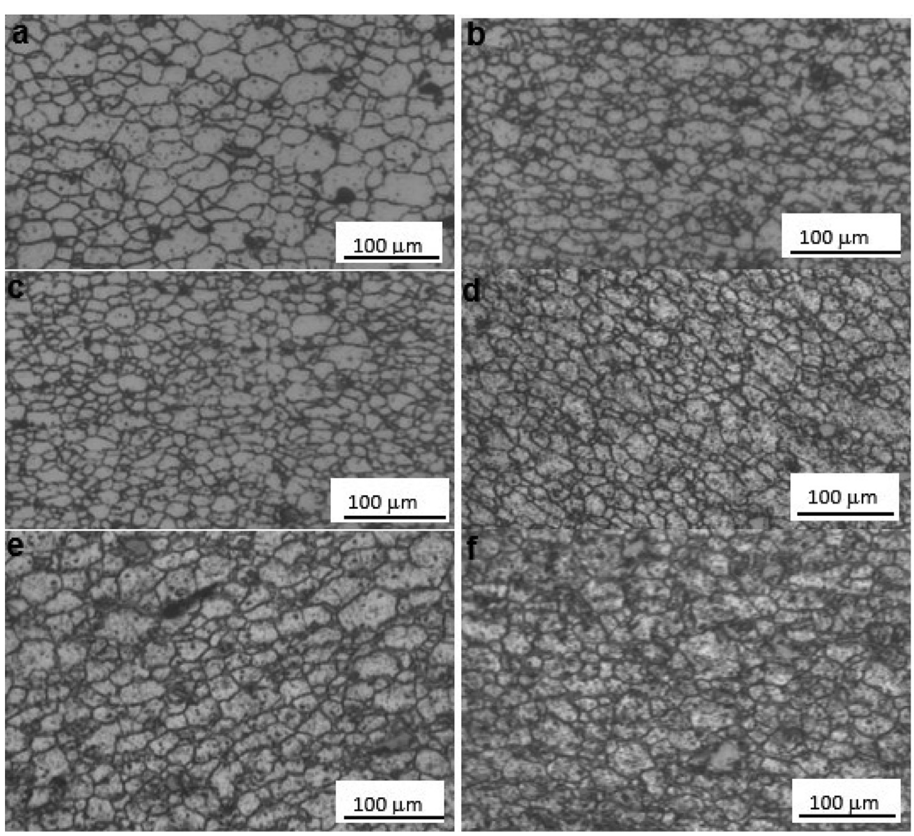

Fig. 3. Microstructure of the SZ: TP1, (a) 1pass- Start, (b) 1pass-Middle, (c) 1pass - End, (d) 2pass - Start, (e) 2pass - Middle and (f) 2pass – End.

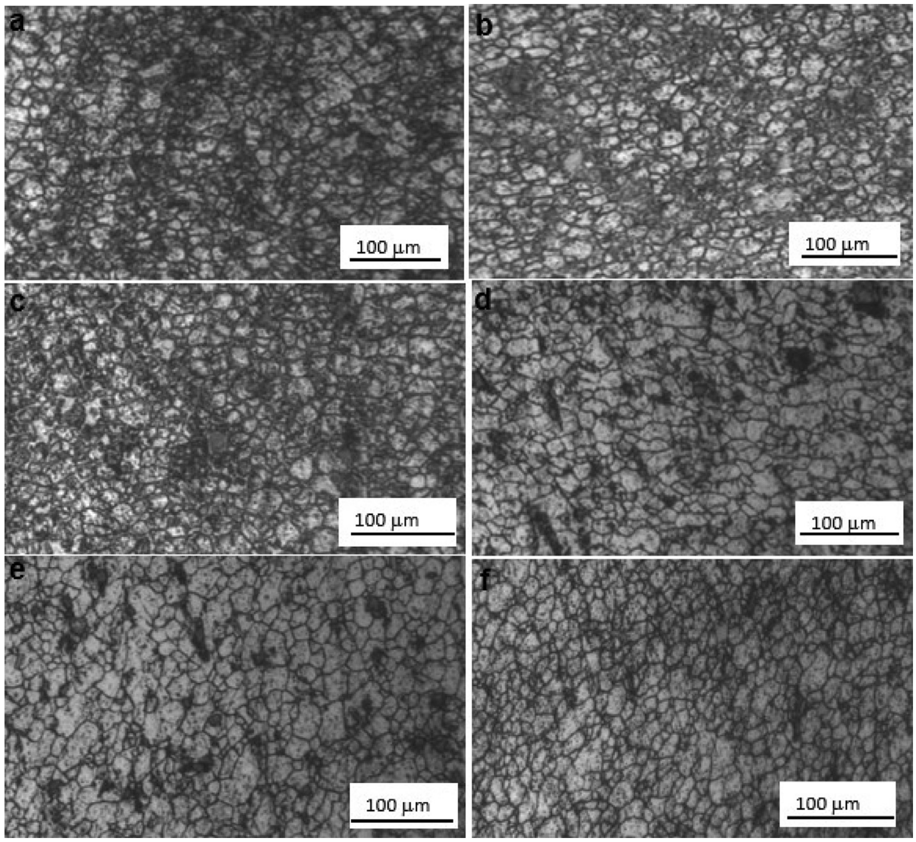

Fig. 4. Microstructure of the SZ: TP2, (a) 1pass- Start, (b) 1pass-Middle, (c) 1pass - End, (d) 2pass - Start, (e) 2pass - Middle and (f) 2pass - End.

the joint. The grains found at the stir zone sampled from the beginning of the joint were coarser compared to grains further from this region. The mean grain size at the stir zone of 2pass SFSP was measured to be between 9.89 μm and 11.97 μm with the maximum mean grain corresponding to the stir zone sampled at the start of the joint and the minimum corresponding to the stir zone sampled at the end of the 2pass SFSP joint. There was a variation in grain size along the joint for both 1pass and 2pass SFSP AA6082/AA8011 joint and this variation is caused by the stability of the heat input along the SFSP joint [13,16,17].

The mean grain size for the 1pass SFSP joint produced using TP2 was found to be in the range of 8.78 μm and 14.78 μm whereas the mean grain size of 2pass ranged between 7.76 μm and 11.59 μm. The same trend observed from the TP1 profile was also observed on joints produced using the TP2 profile. The grains at the stir zone produced using TP2 were finer compared to the stir zone grains produced using TP1. There were no visible pores detected on the stir zone produced using both tool profiles.

3.3. Tensile analysis

The tensile properties of the 1pass and 2pass SFSP AA6082/AA8011 joint produced using TP1 and TP2 pin profiles are summarized in Table 3. The ultimate tensile strength (UTS) and the percentage elongation of the joint sampled from the middle of the plate are higher compared to that of specimens sampled from other locations of the plate for both 1pass and 2pass SFSP joint produced using TP1 profile. This behavior correlates with the grain size measured at the stir zone of the said joint. The UTS of the specimen sampled at the middle of the plate is higher compared to specimens from other locations, however, the increase in UTS compromised the percentage elongation for the 1pass SFSP joint produced using TP2. The 2pass specimen sampled at the end of the plate had the highest UTS and percentage elongation and this specimen was the only specimen with the finest grains at the stir for joint produced using the TP2 profile.

Table 3
Tensile properties of SFSP 1pass and 2pass AA6082/AA8011 dissimilar joint.

Tool profile-pass number	Sampling position	UTS (MPa)	Percentage elongation (%)
TP1-1pass	S	85.8	8.53
	M	90.9	11.35
	E	86.9	11.07
TP1-2pass	S	90.5	22.90
	M	95.3	25.65
	E	93.2	24.37
TP2-1pass	S	92.8	24.04
	M	93.1	22.64
	E	91.9	24.02
TP2-2pass	S	94.8	24.13
	M	95.4	22.10
	E	97.9	25.76

3.4. Fracture mechanism

The fractured surfaces of 1pass and 2pass SFSP AA6082/AA8011 joint produced using the TP1 profile are shown in Fig. 5(a)-(f). Fig. 6 (a)–(f) depicts the fractured morphology of 1pass and 2pass SFSP AA6082/AA8011 joint produced using TP2 profile. The dimpled surfaces are clearly visible from Fig. 5(a), (b), (e), Fig. 6(a)-(f). These dimpled surfaces characterize the ductile failure mode and they

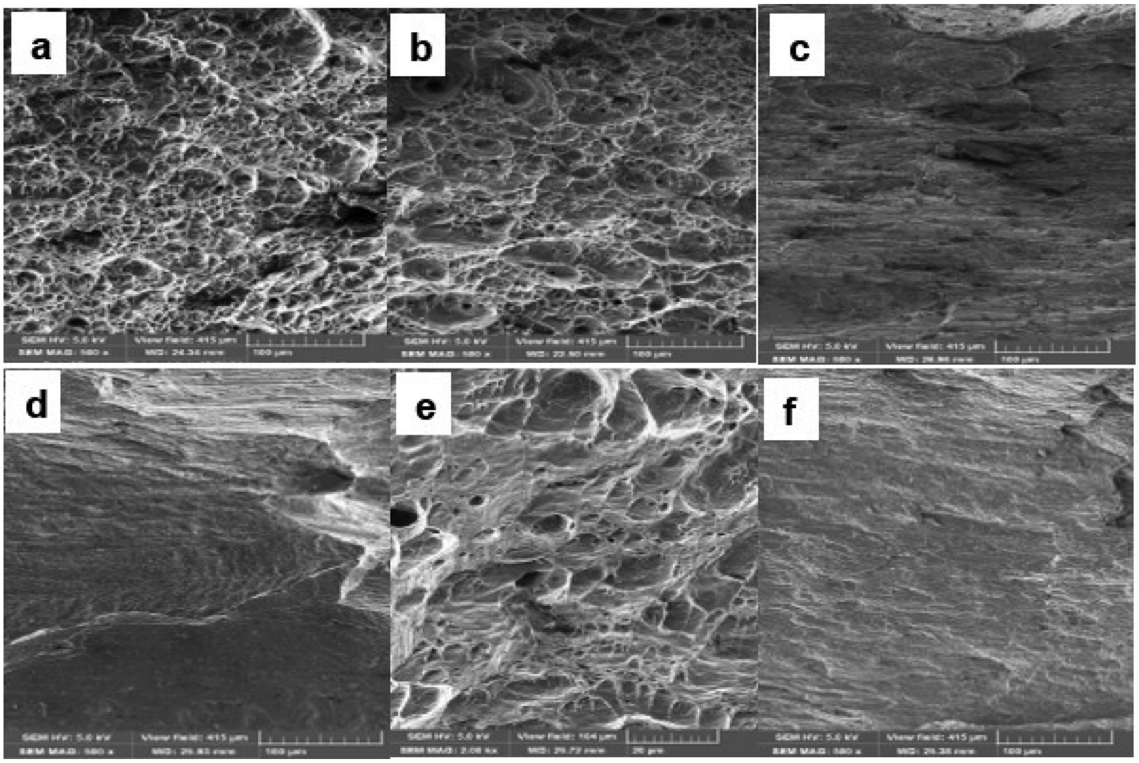

Fig. 5. SEM images:TP1, (a) 1pass - Start, (b) 1pass - Middle, (c) 1pass - End, (d) 2pass – Start, (e) 2pass – Middle, (f) 2pass – End.

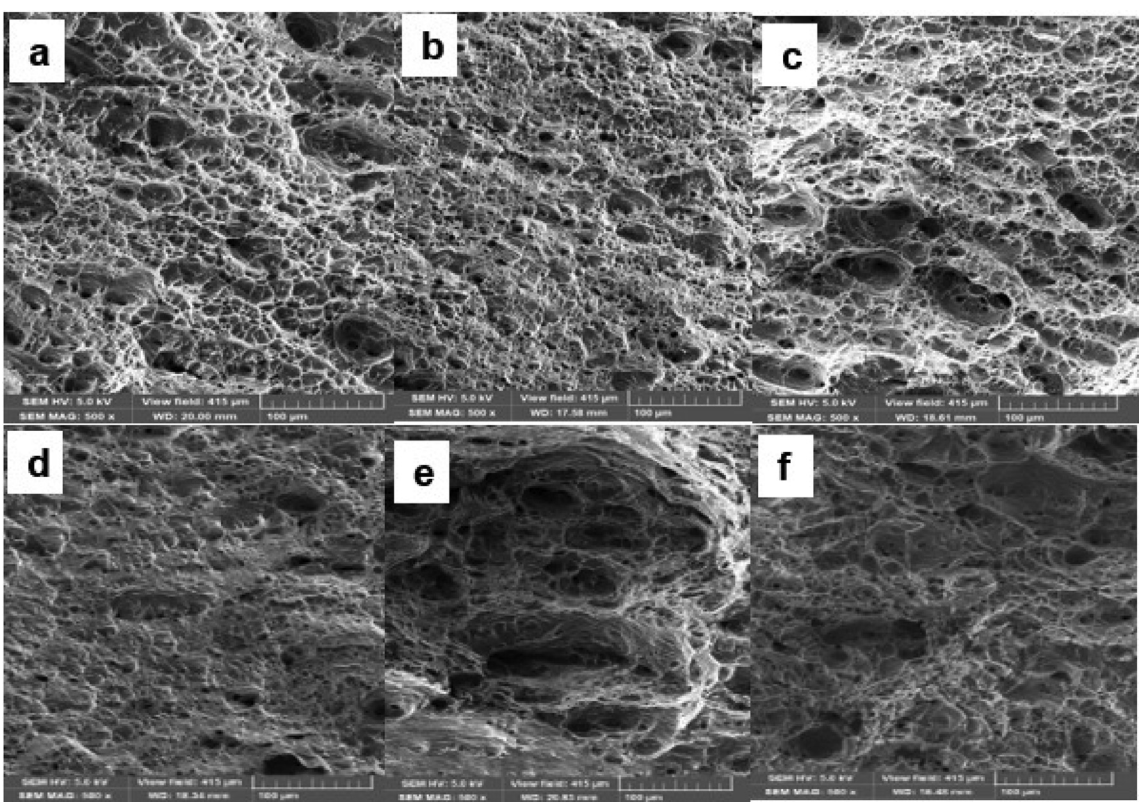

Fig. 6. SEM images:TP2, (a) 1pass - Start, (b) 1pass - Middle, (c) 1pass - End, (d) 2pass – Start, (e) 2pass – Middle, (f) 2pass – End.

are also a confirmation of good material flow that occurred during FSP [16,18,19]. Fig. 5(c), (d), and (f) are the only surfaces with a flat appearance that indicates the cleavage failure mode, and this type of failure is associated with low ductility [17].

3.5. Microhardness analysis

The microhardness of 1pass and 2pass SFSP AA6082/AA8011 joint produced using TP2 is presented in Fig. 7(a) & (b). Fig. 7(c)

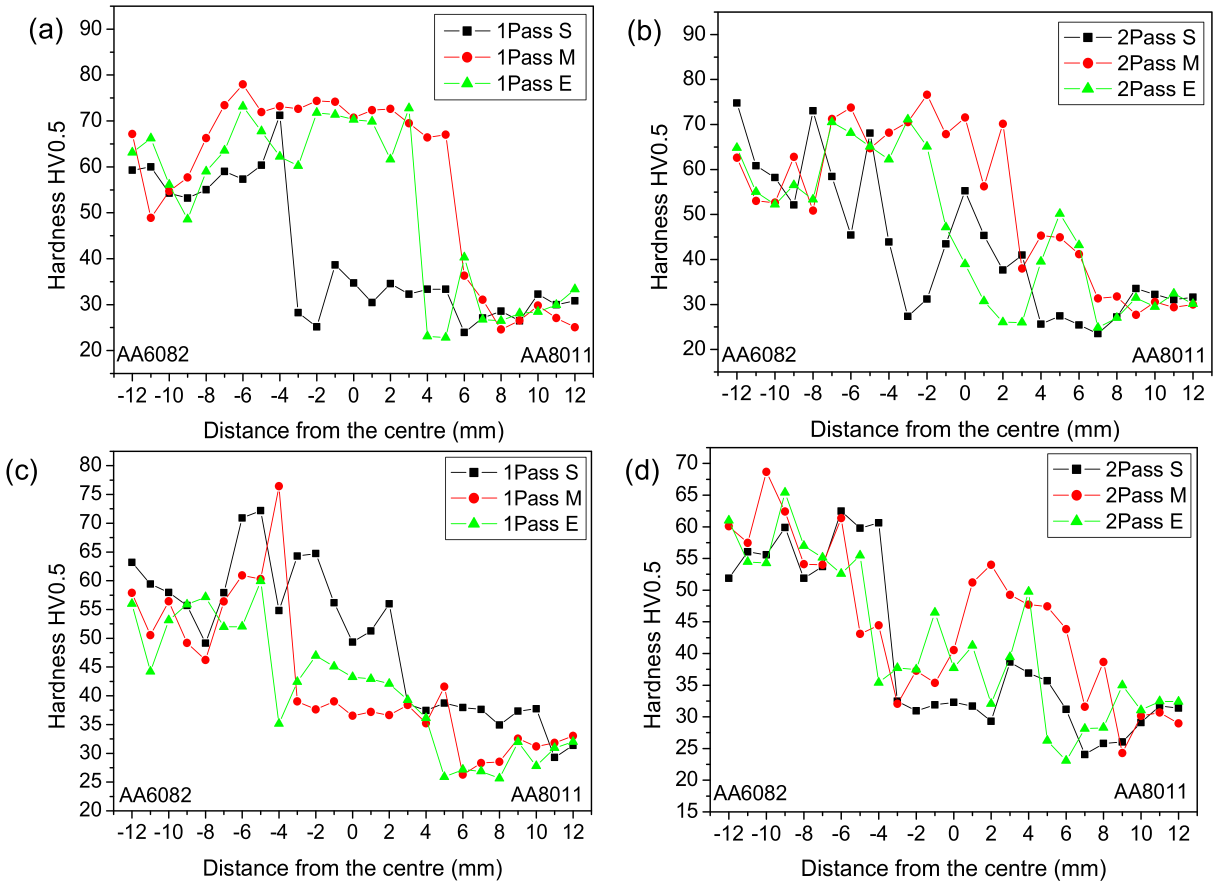

Fig. 7. Microhardness profiles: TP2, (a) 1pass - Start, Middle and End, (b) 2pass – Start, Middle, and End; TP1, (a) 1pass - Start, Middle and End, (b) 2pass – Start, Middle, and End.

& (d) depicts the 1pass and 2pass SFSP AA6082/AA8011 joint produced using TP1. All the microhardness profiles show the declining trend from the AA6082 towards the AA8011 side. However, the microhardness of 1pass and 2pass at the stir zone produced using TP2 is higher compared to other zones of the specimen and this is attributed to the grain size distribution in the stir zone. The higher microhardness also indicates the good material mixing at the stir zone [18]. The microhardness of the stir zone for specimen sampled at the middle of the plate is higher compared to other specimens and this is in correlation to the grain size that was found to be smaller than the other specimens sampled from different locations of the plate. A similar trend observed from the joint produced using TP2 is also observed from the joints produced using TP1. The coarseness of the grains reduces the microhardness of the joint hence the specimens sampled from the start of the joint show low declining trend across the stir zone. It is important to note that the microhardness at the stir zone of joints produced using TP2 is higher compared to that of the joint produced using TP1. The microhardness behavior correlates with the grain distribution that was observed during microstructural analysis.

4. Conclusion

The underwater friction stir processing using two different tool profiles was performed successfully. The mechanical properties of the joints produced using two tool profiles were studied comparatively. The grain size of the joint varies along the joint and this was common on both joints produced using two tool profiles. However, the grain size at the stir zone for the joint produced using the TP2 tool profile was finer compared to that produced using the TP1 tool profile. The joint with fine grains exhibit improved tensile properties compared to that with coarse grains. The joint with low ductility was characterize with cleavage failure mode which indicates the presence of defects at the joint. Moreover, the joint produced using the TP2 profile performed better than the joint produced using the TP1 tool profile.

CRediT authorship contribution statement

Velaphi Msomi: Conceptualization, Supervision, Writing - original draft. **Sipokazi Mabuwa:** Data curation, Formal analysis. **Oritonda Muribwathoho:** Investigation, review & editing. **Sharon S. Motshwanedi:** Validation, Project administration.

Declaration of Competing Interest

The authors would like to confirm that there is no potential conflict of interest that may arise from this work.

Acknowledgments

Special gratitude also goes to the Cape Peninsula University of Technology for unlimited access to the respective equipment needed for the study. The authors would like to thank National Research Foundation for financial support through Thuthuka Grant [118046].

References

[1] R. Senthilkumar, M. Prakash, N. Arun, A.A. Jeyakumar, The effect of the number of passes in friction stir processing of aluminum alloy (AA6082) and its failure analysis, Appl. Surf. Sci. 491 (2019) 420–431, https://doi.org/10.1016/j.apsusc.2019.06.132.

[2] C. Chanakyan, S. Sivasankar, M. Meignanamoorthy, M. Ravichandran, T. Muralidharan, Experimental investigation on influence of process parameter on friction stir processing of AA6082 using response surface methodology, Mater. Today Proc. 21 (2020) 231–236, https://doi.org/10.1016/j.matpr.2019.05.384.

[3] S. Mabuwa, V. Msomi, Comparative analysis between normal and submerged friction stir processed friction stir welded dissimilar aluminum alloy joints, J. Mater. Res. Technol. 9 (5) (2020) 9632–9644.

[4] J.J. Pang, F.C. Liu, J. Liu, M.J. Tan, D.J. Blackwood, Friction stir processing of aluminum alloy AA7075: Microstructure, surface chemistry and corrosion resistance, Corros. Sci. 106 (2016) 217–228.

[5] B. Darras, E. Kishta, Submerged friction stir processing of AZ31 Magnesium alloy, Mater. Des. 47 (2013) 133–137, https://doi.org/10.1016/j.matdes.2012.12.026.

[6] S. Mabuwa, V. Msomi, The effect of friction stir processing on the friction stir welded AA1050-H14 and AA6082-T6 joints, Mater. Today Proc. 26 (2020) 193–199, https://doi.org/10.1016/j.matpr.2019.10.039.

[7] A. MOAREF, A. RABIEZADEH, Microstructural evaluation and tribological properties of underwater friction stir processed CP-copper and its alloy, Trans. Nonferrous Met. Soc. China 30 (4) (2020) 972–981, https://doi.org/10.1016/S1003-6326(20)65269-4.

[8] B. Mirshekari, A. Zarei-Hanzaki, A. Barabi, H.R. Abedi, S.J. Lee, H. Fujii, An anomalous effect of grain refinement on yield stress in friction stir processed lightweight steel, Mater. Sci. Eng. A 799 (2021) 140057, https://doi.org/10.1016/j.msea.2020.140057.

[9] H. Seifiyan, M. Heydarzadeh Sohi, M. Ansari, D. Ahmadkhaniha, M. Saremi, Influence of friction stir processing conditions on corrosion behavior of AZ31B magnesium alloy, J. Magnesium Alloys 7 (4) (2019) 605–616, https://doi.org/10.1016/j.jma.2019.11.004.

[10] S. Bharti, V. Dutta, S. Sharma, N.D. Ghetiya, Investigating the effect of tool speed on the mechanical properties of Al5052 processed by friction stir processing, Mater. Today Proc. 33 (2020) 1605–1609, https://doi.org/10.1016/j.matpr.2020.05.547.

[11] A. Joe Alex, R. Vaira Vignesh, R. Padmanaban, M. Govindaraju, Effect of heat treatment on the mechanical and wear behavior of friction stir processed AA5052 alloy, Mater. Today Proc. 22 (2020) 3340–3346, https://doi.org/10.1016/j.matpr.2020.03.297.

[12] C.Y. Ma, L. Zhou, R.X. Zhang, D.G. Li, F.Y. Shu, X.G. Song, Y.Q. Zhao, Enhancement in mechanical properties and corrosion resistance of 2507 duplex stainless steel via friction stir processing, J. Mater. Res. Technol. 9 (4) (2020) 8296–8305, https://doi.org/10.1016/j.jmrt.2020.05.057.

[13] A. Kumar. Optimization of process parameter for AA6061 alloy during friction stir processing. Mater Today Proc. 2020; Available from http://www.sciencedirect.com/science/article/pii/S2214785320301826.

[14] V. Msomi, N. Mbana. Mechanical properties of friction stir welded AA1050-H14 and AA5083-H111 joint: Sampling aspect. Metals (Basel). 2020;10(2).

[15] F. Baratzadeh, E. Boldsaikhan, R. Nair, D. Burford, H. Lankarani, Investigation of mechanical properties of AA6082-T6/AA6063-T6 friction stir lap welds, J. Adv. Join. Process. 1 (2020). http://www.sciencedirect.com/science/article/pii/S2666330920300091 100011.

[16] H. Kumar, R. Prasad, P. Kumar, S.P. Tewari, J.K. Singh, Mechanical and tribological characterization of industrial wastes reinforced aluminum alloy composites fabricated via friction stir processing Available from J. Alloy. Compd. 831 (2020). http://www.sciencedirect.com/science/article/pii/S0925838820311956 154832.

[17] X.L. Feng, H.J. Liu, J.C. Lippold, H.J. Zhang, H.J. Liu, L. Yu, et al., Influence of multi-pass friction stir processing on microstructure and mechanical properties of 7B04-O Al alloy, Mater. Sci. Eng. A 113 (4) (2013) 789–796.

[18] S. MD, A.K. Birru, Mechanical and metallurgical properties of friction stir welded dissimilar joints of AZ91 magnesium alloy and AA 6082-T6 aluminium alloy, J. Magnesium Alloys 7 (2) (2019) 264–271, https://doi.org/10.1016/j.jma.2018.09.004.

[19] P. Cavaliere, A. De Santis, F. Panella, A. Squillace, Effect of welding parameters on mechanical and microstructural properties of dissimilar AA6082–AA2024 joints produced by friction stir welding, Mater. Des. 30 (3) (2009) 609–616, https://doi.org/10.1016/j.matdes.2008.05.044.